

Mode locking via delayed orthogonal-polarization reinjection in semiconductor lasers

T. Wang¹, Y. Ma¹, Z. Li¹, Y. Li¹, Z. Tu¹, Y. Zhang¹, G. Xu², S. Baland³, S. Xiang¹, Y. Hao⁴

¹*State Key Laboratory of Integrated Service Networks,*

School of Telecommunications Engineering, Xidian University, Xi'an 710071, China

²*School of Optical and Electronic Information & Wuhan National Laboratory for Optoelectronics, Huazhong University of Science and Technology, 1037 Luoyu Road, Wuhan 430074, China*

³*Université Côte d'Azur, Institut de Physique de Nice, UMR 7010 CNRS, Nice, 06200, France and*

⁴*State Key Discipline Laboratory of Wide Bandgap Semiconductor Technology, School of Microelectronics, Xidian University, Xi'an 710071, China*

(Dated: April 17, 2025)

We demonstrate harmonic mode-locking in a semiconductor laser using orthogonal-polarization reinjection via an external ring cavity integrated with a rotatable $\lambda/2$ -plate. By tuning the plate angle θ , we achieve precise control over pulse multiplicity and repetition rates in orthogonal TE/TM modes. For the TE mode, increasing θ transitions the system from low amplitude and disordered quasi-periodic states to fundamental (single-pulse) mode locking and harmonic dual-pulse regimes. Polarization resolved measurements and cross-correlation analyses reveal polarization-mediated dynamics, achieving coherent pulse alignment at half the cavity roundtrip time. This work establishes orthogonal polarization feedback as a compact, versatile mechanism for tailoring ultrafast pulse trains, enabling applications in polarization-multiplexed communications, dual-comb spectroscopy, and high-repetition-rate photonic systems.

PACS numbers:

INTRODUCTION

In recent years, mode locking has been considered as a cornerstone technique for generating ultrashort optical pulses with repetition rates ranging from MHz to GHz [1, 2]. This capability provides promising platforms for fundamental research and various applications, including optical telecommunications, spectroscopy, material processing and neuromorphic computing. [3–6]. Consequently, the investigation of mode locking in semiconductor lasers has garnered significant attention from researchers.

Mode locking is a resonant process that generates pulsed radiation by synchronizing the phases of multiple longitudinal modes within the resonator [7]. Typically, it can be achieved actively [8] or passively [9, 10]. For active mode locking, the laser resonator incorporates an active element that modulates the output. Specifically, an electro-optic modulator or a Mach-Zehnder optical modulator, synchronized with the laser's round-trip, can generate short pulses [11]. On the other hand, passive mode-locking doesn't need for any external modulation, making it the preferred method for generating optical pulses at multi-GHz repetition rates [12]. Passive mode locking is typically achieved by integrating two key components: a laser amplifier that supplies gain and a saturable absorber that functions as a pulse-shortening element [13].

Apart from inserting a saturable absorber [14], crossed-polarization gain modulation method was proposed to achieve passive mode-locking for semiconductor lasers [4]. However, experimental validation of this concept in its most straightforward implementation

remains elusive. In this paper, we demonstrate harmonic mode-locking in semiconductor lasers via orthogonal polarization feedback, a paradigm distinct from conventional methods. By exciting TE and TM modes with the feedback loop and tuning the feedback phase, we achieve synchronized pulse generation in both polarizations, with repetition rates governed by the cavity roundtrip time. Our results establish cross-polarization feedback as a versatile tool for ultrafast pulse engineering, with direct applications in coherent optical communications and photonic neuromorphic systems. By bridging a new experiment with existing theory [4], this work opens new avenues for designing compact, polarization-multiplexed ultrafast sources.

EXPERIMENTAL SETUP

The top panel of Fig. 1 illustrates the experimental arrangement for our investigation. This configuration employs a semiconductor VCSEL (Thorlabs L850VH1) with emission wavelength $\lambda = 850$ nm, and which is stabilized at 25°C by a temperature controller (Thorlabs TED200C). The VCSEL operates in a single longitudinal and transverse mode, as well as in one of two orthogonal linear polarization modes, and is driven by a low-noise current source (Thorlabs LDC205C).

After passing through a 50:50 beam splitter (BS), the laser light is sent to an external ring cavity, which can reflect the light back. A polarizing beam splitter (PBS) and a $\lambda/2$ plate are placed within the external cavity. Inside the cavity, the PBS separates the TE and TM modes, which then can undergo up to 90-degree

rotation after passing through the $\lambda/2$ plate. The second arm exiting the first BS is directed towards another PBS for detection. Both TE and TM outputs of the PBS are directed towards optical isolators and finally two AC-coupled and 10 GHz - bandwidth amplified fast detectors (PD2 and PD3). The temporal signals are then monitored using a 20 GHz oscilloscope (Tektronix DSA72004) with a sampling rate of 50 GHz. The total feedback length within the system is 1.8 meters, corresponding to a round-trip time of approximately 12 ns.

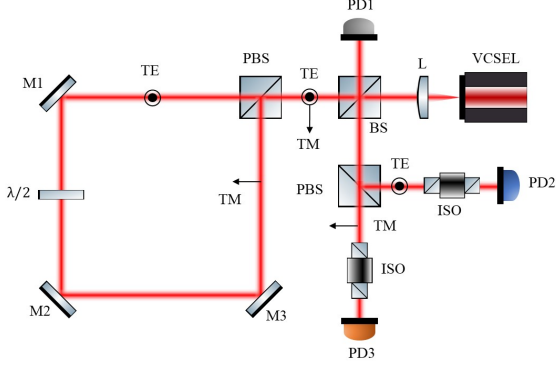


FIG. 1: Experimental setup: VCSEL, Vertical Cavity Surface Emitting Laser; L, optical lens; BS, beam splitter; PBS, polarized beam splitter; M, mirror; $\lambda/2$, half-wave plate; ISO, optical isolator; PDn, photodetectors; Osc., oscilloscope.

RESULTS AND DISCUSSIONS

Fig. 2a shows the polarization-resolved input-output function curves of the free running laser, which indicate the distinct lasing behaviors of the TE and TM modes. In particular, the TE mode has a much smaller threshold than the TM mode [15]: $J_{th}^{TE} \approx 1.48 \text{ mA}$ versus $J_{th}^{TM} \approx 5.20 \text{ mA}$. In the intermediate current regime ($J_{th}^{TE} < J < J_{th}^{TM}$), the output of the TE mode linearly increases with injection current (red curve), while the power of the TM mode remains almost zero (light blue curve). The TM mode starts to be lasing when $J > J_{th}^{TM}$, and polarization dynamics is observed for both modes. The orange-shaded region near J_{th}^{TM} holds particular significance, as enhanced orthogonal-polarization gain modulation in this regime – consistent with theoretical frameworks [4, 16] – creates favorable conditions for passive mode-locking through nonlinear polarization coupling [17].

Fig. 2b shows the variation in the feedback light power (measured by the power meter PD1) as a function of the angle of the $\lambda/2$ -plate (θ) at $J = 5.30 \text{ mA}$. More information can be found in the polarization-resolved time-averaged intensities, which show that the intracavity nonlinear interaction induces distinct mode-selective responses: (i) the TE-mode output (measured

by a power meter in the location of PD2) remains constant at $650 \mu\text{W}$ for $\theta < 45^\circ$ which indicates that up to that angle, the reinjection has very moderate effect on the time-averaged TE intensity. At higher angles the time-averaged TE intensity grows by up to 5% increase, peaking at $\theta < 65^\circ$ (Fig. 2c), suggesting constructive interference in dominant polarization channel; (ii) the TM-mode output (measured at the location of PD3) conversely exhibits in-phase modulation with feedback signal but at much lower intensity (Fig. 2d), indicative of weak cross-polarization coupling. These observations highlight the critical role of polarization-state matching in governing nonlinear mode competition dynamics.

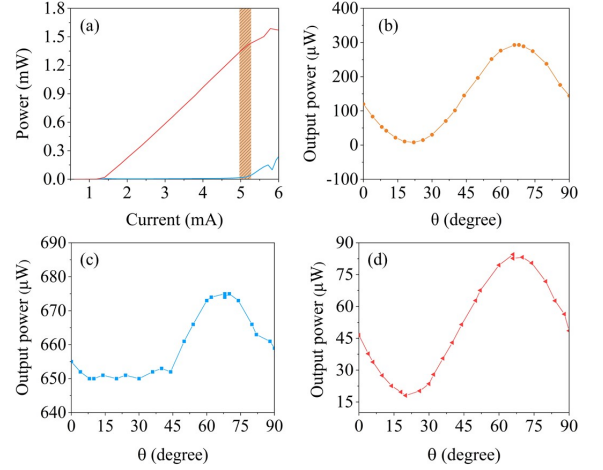


FIG. 2: Fundamental characterizations of the the VCSEL under free running and with external feedback: (a) input-output function curves of the TE and TM modes as a function of pump current. The red curve indicates the TE mode, and the light blue curve denotes the TM mode; (b) averaged power of the feedback light, measured at 5.30 mA, after circulating from the ring cavity; (c) and (d), output powers of the TE and TM modes at $J = 5.30 \text{ mA}$ after the injection of the feedback light.

Fig. 3 presents the spatio-temporal diagrams and typical dynamics of the TE mode under a bias current of $J = 5.30 \text{ mA}$ with θ values of 50° , 60° and 70° , respectively. It is clear that the $\lambda/2$ -plate plays significant role on the mode dynamics. At $\theta = 50^\circ$ (Fig. 3a), a weakly modulated periodic pattern appears, characterized by small-amplitude oscillations within each roundtrip (T_{rt}), as shown by the bottom panel of Fig. 3a. Increasing θ to 60° (Fig. 3b) triggers a fundamental mode-locking state, where a single pulse is stably confined per roundtrip (bottom panel of Fig. 3b). The symmetric single-pulse locking may come from balanced nonlinear phase shifts and gain-loss equilibrium, enabled by the plate's orientation [18, 19].

Further increasing $\theta = 70^\circ$ (Fig. 3b) results in dual-pulse locking within one roundtrip T_{rt} . The asymmetry of the pulses as measured by the AC-coupled detectors

suggest slightly different rising and falling slopes. We underline that very precise tuning of the half-wave plate is required to reach this regime, suggesting the key role of precise feedback phase. As we discuss later on, this is a case of harmonic mode-locking since both pulses are evenly distributed within one roundtrip, so that the period of this solution is exactly half that of the fundamental mode-locked state. These transitions demonstrate the critical role of the $\lambda/2$ -plate in regulating pulse formation and stability in the TE mode.

Fig. 4 exhibits the corresponding spatio-temporal diagrams and representative dynamics of the TM mode under the same bias current and the same angles of the $\lambda/2$ -plate with the TE mode, respectively. At $\theta = 50^\circ$ (Fig. 4a), the periodic structure is less pronounced compared to the TE mode, though visible temporal features emerge within a single roundtrip (bottom panel). Increasing θ to 60° (Fig. 4b) stabilizes a harmonic mode-locking state, where two asymmetric pulses (left pulse stronger than the right) are confined per roundtrip - a notable contrast to the single-pulse locking observed in the TE mode (bottom panel of Fig. 4b). Besides, we also observe that both pulses exhibit significantly weaker peak amplitudes than their TE counterparts (lower panel).

Further increasing θ to 70° leads to stable dual-pulse locking, but with comparable amplitudes (Fig. 4c), mirroring the TE mode's behavior at this angle. Obviously, the amplitudes of both pulses are much weaker the bottom panel of Fig. 4c, highlighting mode-specific nonlinear absorption.

Further insight can be gained by comparing autocorrelation of each polarization and cross-correlation between both, as shown on Fig. 5. Specifically, Fig. 5a-c show the autocorrelation traces of the TE mode with $\lambda/2$ -plate angle $\theta = 50^\circ, 60^\circ$, and 70° . At $\theta = 50^\circ$ (Fig. 5a), the trace features a prominent central peak at zero delay with a few irregular sidebands up to 12.4 ns. These features are consistent with the quasi-periodic and weakly modulated patterns in the spatio-temporal representation in Fig. 3a. Increasing θ to 60° (Fig. 5b), leads to disappearance of the sidebands, leaving only a single secondary peak at 12.3 ns (roundtrip time) which shows fundamental mode-locking with one pulse per roundtrip. At $\theta = 70^\circ$ (Fig. 5c), the autocorrelation shows the emergence of a secondary peak at half the round-trip time. The absence of any other feature in the autocorrelation confirms the harmonic locking situation.

Fig. 5d-f show the TM mode's autocorrelation traces under identical θ values. The TM mode exhibits weaker amplitudes ($\sim 30\%$) and an elevated noise floor, attributed to polarization-dependent losses and mode competition, in agreement with the time-averaged intensities in Fig. 2. At $\theta = 50^\circ$ (Fig. 5d), broadened peaks and suppressed sidebands indicate polarization-filtered gain saturation, attenuating

nonlinear interactions. For $\theta = 60^\circ$ (Fig. 5e), two feedback signatures emerge: a primary peak at 12.3 ns and a weaker peaks at 6.1 ns and 18.4 ns, suggesting harmonic mode-locking and emergence of TM-specific cavity instabilities. At $\theta = 70^\circ$ (Fig. 5f), harmonic mode-locking becomes clear, with periodic peaks spaced by 6.15 ns and uniform amplitudes, reflecting symmetrical dual-pulse circulation stabilized by polarization-optimized phase matching.

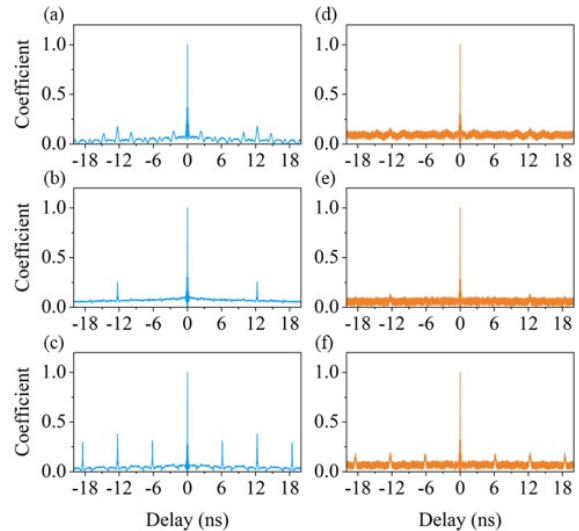


FIG. 5: Autocorrelation coefficients calculated by using the temporal signals of the TE and TM mode with different $\lambda/2$ -plate angles: (a)-(c) for TE mode; (d)-(f) for TM mode. (a) and (d) for 50° ; (b) and (e) for 60° ; (c) and (f) for 70° .

To further understand the polarization-dependent mode-locking dynamics, we calculated the cross-correlation traces between TE and TM modes at $\lambda/2$ -plate angle $\theta = 60^\circ$ and 70° . As shown by Fig. 6a, at $\theta = 60^\circ$, the cross-correlation coefficient exhibits a weak anti-correlation between the two polarization modes near zero delay with periodic side peaks. These features are superimposed on a pronounced noise floor, reaching $\sim 40\%$ of the central peak amplitude, suggesting partially randomized mode coupling. The bimodal amplitude distribution—sharp higher-amplitude peaks (TE-dominated pulses) alternating with suppressed lower-amplitude peaks (TM-dominated)—reflects asymmetric nonlinear coupling dynamics. This asymmetry stems from polarization-dependent gain saturation that selectively amplifies the TE mode, effectively suppressing TM mode oscillations. The observed ~ 6.15 ns temporal separation between adjacent peaks further suggests periodic energy exchange between polarization states during pulse evolution.

Increasing θ to 70° (Fig. 6b) sharpens the cross-correlation profile: the anti-correlation deepens (minimum ~ -0.1), while periodic peaks emerge

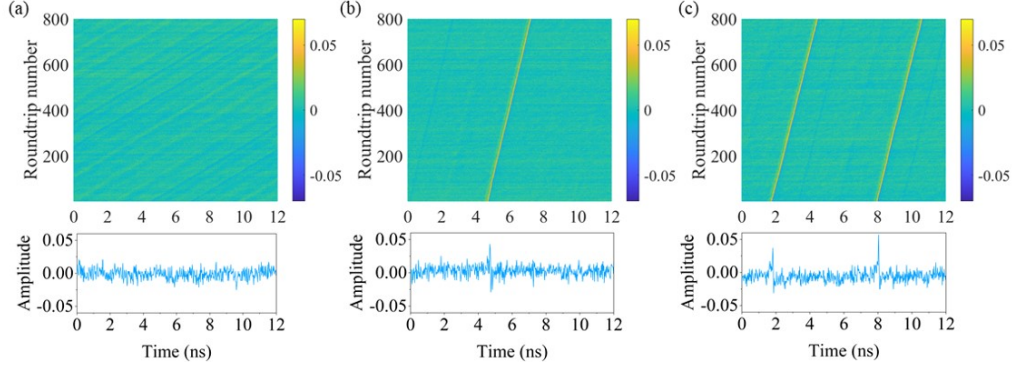


FIG. 3: Spatio-temporal diagrams and temporal dynamics of the TE mode in the laser output under a bias current $J = 5.30\text{mA}$, with $\lambda/2$ -plate angles $\theta = 50^\circ$, 60° and 70° , respectively.

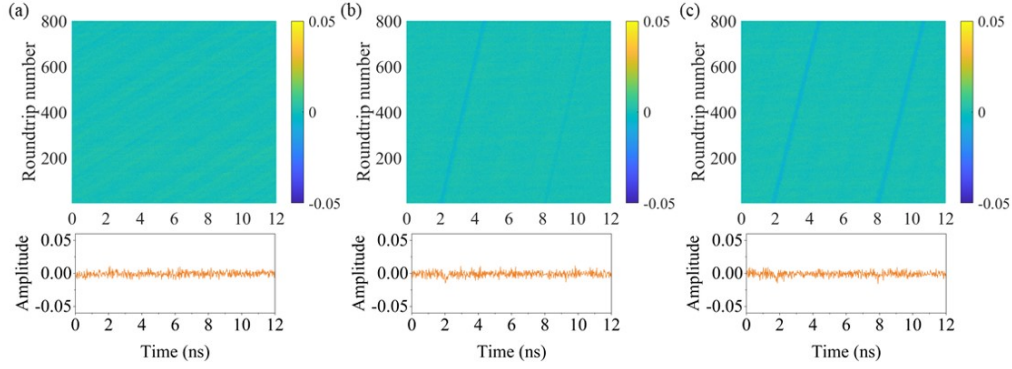


FIG. 4: Corresponding spatio-temporal diagrams and temporal dynamics of the TM mode in the laser output under a bias current $J = 5.30\text{mA}$, with $\lambda/2$ -plate angles $\theta = 50^\circ$, 60° and 70° , respectively.

at $\pm 6.15\text{ ns}$ intervals – exactly half the cavity roundtrip time. At this angle, the $\lambda/2$ -plate optimizes polarization alignment, enabling cross-polarization nonlinearities to synchronize TE and TM pulses. The halved periodicity corresponds to subharmonic locking, where two temporally aligned pulses per roundtrip (one TE- and one TM-dominated) form a stable composite waveform. This dual-pulse locking is mediated by intensity-dependent birefringence, which dynamically compensates group velocity mismatch during propagation. The transition disordered anti-correlation at 60° to periodic harmonic locking at 70° underscores the critical role of polarization control in achieving coherent multipulse interactions.

CONCLUSIONS

In conclusion, we have presented an experimental demonstration of fundamental and harmonic mode-locking in semiconductor lasers induced by crossed-polarization gain modulation. In our scheme, by rotating the $\lambda/2$ -plate, we can precisely control over pulse multiplicity, symmetry, and temporal coherence in both TE and TM modes. The TE mode transitions

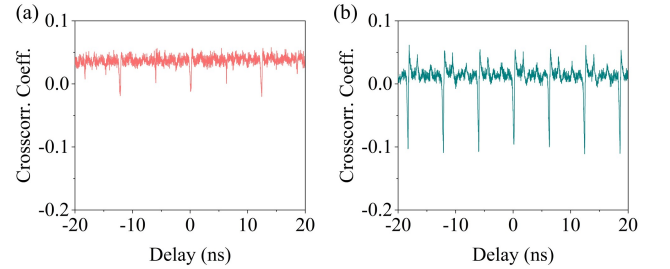


FIG. 6: Cross-correlation coefficients calculated by using the temporal signals of the TE and TM mode with different $\lambda/2$ -plate angles: (a) 60° ; (b) 70° .

from weakly modulated quasi-periodic states ($\theta = 50^\circ$) to harmonic mode-locking ($\theta = 60^\circ$) and dual-pulse regimes ($\theta = 70^\circ$), while the TM mode exhibits subharmonic locking and intermittent dynamics, highlighting polarization-divergent nonlinearities. The ability to independently tailor TE and TM pulse trains via a single $\lambda/2$ -plate enables polarization-multiplexed ultrafast sources, critical for dual-comb spectroscopy and optical communications. The observation of harmonic locking regimes (half roundtrip time) opens avenues

for high-repetition-rate pulse generation without cavity shortening, leveraging polarization-driven pulse splitting. Thus, our study mark a pivotal step toward on-demand pulse shaping in integrated photonic systems, where polarization degrees of freedom can unlock unprecedented functional scalability.

Acknowledgment

This work is partially supported by National Natural Science Foundation of China (Grant No. 62475206 and 61804036), Key Research and Development Plan of Shaanxi Province of China (Grant No. 2024GH-ZDXM-42), National Key Research and Development Program of China (Grant No. 2021YFB2801900, 2021YFB2801901, 2021YFB2801902, and 2021YFB2801904).

-
- [1] A. Gordon and B. Fischer, Physical review letters **89**, 103901 (2002).
 - [2] U. Keller and R. Paschotta, *Ultrafast lasers* (Springer, 2021).
 - [3] E. Avrutin, J. Marsh, and E. Portnoi, IEE Proceedings-Optoelectronics **147**, 251 (2000).
 - [4] J. Javaloyes, J. Mulet, and S. Balle, Physical review letters **97**, 163902 (2006).
 - [5] A. Aadhi, I. Alamgir, L. Di Lauro, B. Fischer, N. Perron, P. Dmitriev, C. Mazoukh, P. Roztock, C. Rimoldi, M. Chemnitz, et al., APL Photonics **9** (2024).
 - [6] J. P. von der Weid, M. M. Correia, P. Tovar, A. S. Gomes, and W. Margulis, Nature Communications **15**, 177 (2024).
 - [7] L. Zhan, Z. Gu, J. Zhang, and Y. Xia, Optics letters **32**, 2276 (2007).
 - [8] D. Revin, M. Hemingway, Y. Wang, J. Cockburn, and A. Belyanin, Nature Communications **7**, 11440 (2016).
 - [9] M. Marconi, J. Javaloyes, S. Balle, and M. Giudici, Physical review letters **112**, 223901 (2014).
 - [10] A. Fülöp, M. Mazur, A. Lorences-Riesgo, Ó. B. Helgason, P.-H. Wang, Y. Xuan, D. E. Leaird, M. Qi, P. A. Andrekson, A. M. Weiner, et al., Nature communications **9**, 1598 (2018).
 - [11] Y. Zhang, J. Li, C. Meng, S. Li, Z. Zeng, L. Zhang, Z. Zhang, S. Zhang, and Y. Liu, Journal of Lightwave Technology (2024).
 - [12] A. Yadav, N. B. Chichkov, E. A. Avrutin, A. Gorodetsky, and E. U. Rafailov, Progress in quantum electronics **87**, 100451 (2023).
 - [13] M. Marconi, J. Javaloyes, S. Barland, S. Balle, and M. Giudici, Nature Photonics **9**, 450 (2015).
 - [14] S. Ruschel, V. A. Pammi, R. Braive, I. Sagnes, G. Beaudoin, N. G. Broderick, B. Krauskopf, and S. Barbay, Optics Letters **50**, 2618 (2025).
 - [15] T. Wang, H. Zhou, Q. Fang, Y. Han, X. Guo, Y. Zhang, C. Qian, H. Chen, S. Barland, S. Xiang, et al., Chaos, Solitons & Fractals **181**, 114673 (2024).
 - [16] J. Mulet, J. Javaloyes, and S. Balle, IEEE journal of quantum electronics **43**, 786 (2007).
 - [17] M. Fermann, M. Andrejco, Y. Silberberg, and M. Stock, Optics letters **18**, 894 (1993).
 - [18] P. Grelu and N. Akhmediev, Nature photonics **6**, 84 (2012).
 - [19] L. Zhao, D. Tang, X.-h. Wu, H. Zhang, and H. Y. Tam, Optics Letters **34**, 3059 (2009).